The roles of static stability and tropical–extratropical interactions in the summer interannual variability of the North Atlantic sector

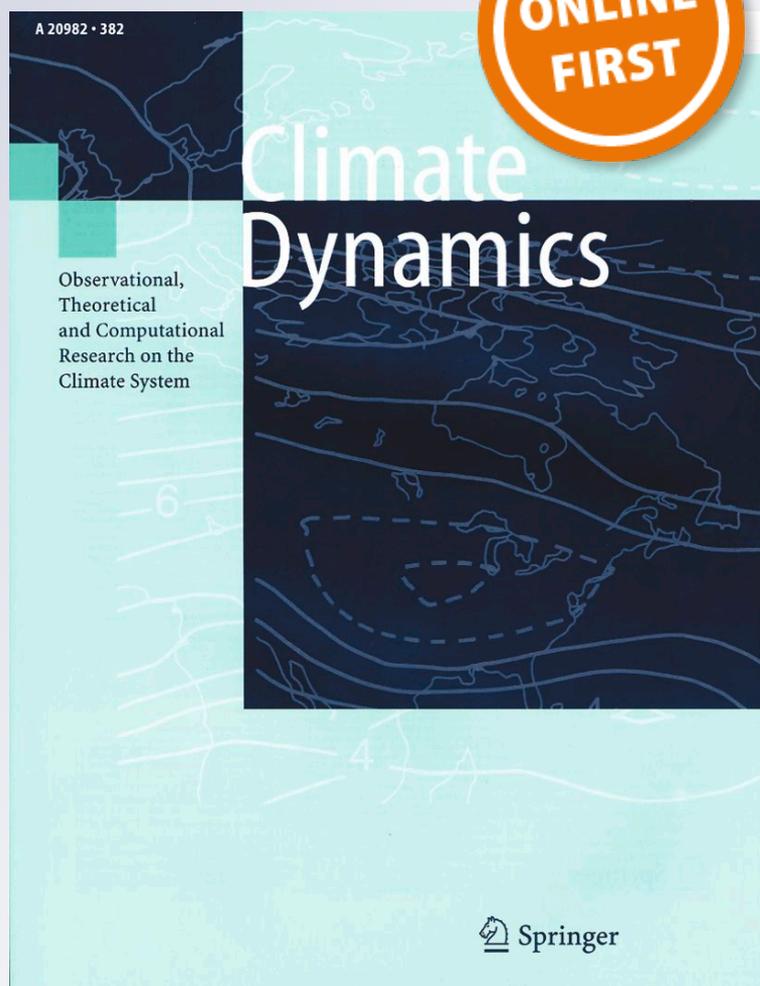## Cheikh Oumar Mbengue, Tim Woollings, Helen F. Dacre & Kevin I. Hodges

A 20982 · 382

Climate Dynamics

Observational, Theoretical and Computational Research on the Climate System

6

4 A

🛡 Springer

ONLINE FIRST

🛡 Springer

Springer

CrossMark

The roles of static stability and tropical–extratropical interactions in the summer interannual variability of the North Atlantic sector

Cheikh Oumar Mbengue[1] · Tim Woollings[1] · Helen F. Dacre[2] · Kevin I. Hodges[2]

Abstract
Summer seasonal forecast skill in the North Atlantic sector is lower than winter skill. To identify potential controls on predictability, the sensitivity of North Atlantic baroclinicity to atmospheric drivers is quantified. Using ERA-INTERIM reanalysis data, North Atlantic storm-track baroclinicity is shown to be less sensitive to meridional temperature-gradient variability in summer. Static stability shapes the sector's interannual variability by modulating the sensitivity of baroclinicity to variations in meridional temperature gradients and tropopause height and by modifying the baroclinicity itself. High static stability anomalies at upper levels result in more zonal extratropical cyclone tracks and higher eddy kinetic energy over the British Isles in the summertime. These static stability anomalies are not strongly related to the summer NAO; but they are correlated with the suppression of convection over the tropical Atlantic and with a poleward-shifted subtropical jet. These results suggest a non-local driver of North Atlantic variability. Furthermore, they imply that improved representations of convection over the south-eastern part of North America and the tropical Atlantic might improve summer seasonal forecast skill.

1 Introduction

Seasonal predictions of some major meteorological variables over the North Atlantic in summer are inferior to those in winter. For example, Wang et al. (2009) used 14 models from the Climate Prediction and its Application to Society (CliPAS) project to show that precipitation and circulation forecasts are generally better during winter—an issue which remains today (various personal communications). This is surprising because the summer extratropics are more baroclinically stable, since meridional temperature gradients are weaker. Weaker baroclinicity implies weaker macroturbulence. In other words, the 'noise' in the signal-to-noise ratio is lower in the summer. Hence, the summertime could be more predictable. But because of stronger tropical–extratropical interactions in winter and also because tropical dynamics are more linear on seasonal timescales,

the wintertime turns out to be more predictable than the summertime (for a review of seasonal forecasting and predictability, see Palmer and Anderson 1994; Hoskins 2013). Therefore, it appears that, on seasonal timescales, external predictable drivers are more important than the inherent predictability of the local flow.

Dynamical differences between seasons could account for the differences in seasonal forecast skill. Indeed, the North Atlantic sector summer circulation differs from the winter circulation in several ways (see White 1982; Mesquita et al. 2008). During summer, for instance, the center of action of the North Atlantic storm track is shifted poleward when compared to the winter. Eddy-energy transports are weaker and synoptic and planetary wave amplitudes are smaller during the summertime (White 1982). Furthermore, some of the characteristics of the cyclones and anticyclones that make up the summer extratropical storm tracks differ (Bengtsson et al. 2006). For example, it has been found that summer cyclones are in general weaker, propagate slower, but live longer than winter ones. Furthermore, climate change simulations using a hierarchy of models show marked differences between summer and winter storm-track responses, as well as seasonal variations in the relative importance of transient and stationary eddies (Simpson et al. 2014; McGraw

✉ Cheikh Oumar Mbengue
  c.mbengue@wolfson.oxon.org

[1] Atmospheric, Oceanic, and Planetary Physics, Sherrington Road, Oxford OX1 3PU, UK

[2] Department of Meteorology, University of Reading, Reading, UK

and Barnes 2016; Baker et al. 2017). Here we investigate whether dynamical differences between the summer and winter North Atlantic sector help to explain seasonal differences in potential predictability. In so doing, we inquire about the sensitivity of baroclinicity to known, predictable drivers.

Extratropical dynamics are mostly shaped by baroclinic eddies. They result from the baroclinically unstable nature of the midlatitude troposphere (Charney 1947; Eady 1949). Because theories of baroclinic instability underpin much of our understanding of midlatitude dynamics, previous authors have analyzed the components of a variety of baroclinicity measures to further our understanding of midlatitude dynamics. , for example, the Eady growth rate (e.g. Yin 2005) and mean available potential energy (MAPE) (e.g. O'Gorman and Schneider 2008; Mbengue and Schneider 2017). In this paper, we test the hypothesis that the amplitude of the extratropical response to known, predictable drivers varies seasonally in part because of differences in the spatial distribution of the sensitivity of MAPE to its components. Also, we investigate how variability in North Atlantic static stability shapes the variability of the North Atlantic sector. We focus explicitly on the role of static stability because previous work has shown that variability in the zonal-mean static stability can modulate the extratropical storm-track response (Mbengue and Schneider 2017).

Section 2 details the data used in this study and describes the methods used in the analysis. Section 3 explicates a relevant theoretical framework. Section 4 presents the results, while Sect. 5 follows with a discussion of those results. The conclusions are outlined in Sect. 6.

2 Data and methods

Data from the European Centre for Medium-range Weather Forecast's (ECMWF) ERA-INTERIM reanalysis (Dee et al. 2011) for boreal winter (DJF) and summer (JJA) periods spanning 1981–2013 were analyzed. The reanalysis's dynamical core solves the primitive equations on a sphere using a spectral transform method at T255 horizontal resolution and with 60 hybrid sigma-pressure vertical levels. This reanalysis is favored because it uses four-dimensional variational data assimilation and has been shown to be an improvement over older reanalyses, such as the ERA40 and NCEP-NCAR reanalyses. Data from the ERA-INTERIM reanalysis is used to compute seasonal-mean statistics of static stability, baroclinic mean available potential energy, the zonal winds, eddy kinetic energy, meridional eddy temperature fluxes, specific humidity, and geopotential height.

Unless otherwise stated, empirical orthogonal functions (EOFs) and their associated principal components (PCs) are evaluated over the region (70W–10W, 20N–60N) in order to isolate the leading modes of variability of the North Atlantic sector. EOFs are computed from linear detrended time series of seasonal means weighted by the factor $\sqrt{\cos \varphi}$, where φ is latitude. Composite climatologies based on the PC time series use years with normalized PC scores above the 75th percentile as the positive phase and years with normalized PC scores below the 25th percentile as the negative phase.

England and Wales daily precipitation data obtained from the UK Met Office Hadley Centre (Alexander and Jones 2001) are used to conduct a lagged correlation between the time series of precipitation over the British Isles and Northeast Atlantic upper-level static stability. Finally, gridded daily outgoing longwave radiation (OLR) data obtained from the NOAA/OAR/ESRL Physical Sciences Division (Liebmann and Smith 1996) are used in correlation analyses to probe tropical–extratropical interactions.

The time series of the NAO is computed using the 1st principal component of 500 hPa geopotential height over the region (75W–15E, 20N–90N) following Woollings et al. (2010).

2.1 Cyclone track statistics

Cyclone track statistics are used to ascertain how individual cyclones interact with North Atlantic upper-level stability anomalies. They are derived from 6-h ERA-INTERIM reanalysis fields that are truncated to T42 spectral resolution to reduce noise. The tracking methodology follows Hoskins and Hodges (2002). The tracking algorithm links identified maxima in 850 hPa vorticity and obtains a smooth path by minimizing a cost function (Hodges 1995, 1999). Valid cyclone tracks must have a maximum relative vorticity exceeding 10^{-5} /s, last for at least 2 days, and travel at least 1000 km. These criteria are designed to capture mobile synoptic scale systems.

2.2 Transient eddy fields

Transient-eddy fields are computed from 2 to 10 day bandpass filtered (Blackmon 1976; Blackmon et al. 1977; Hoskins and Hodges 2002) daily fields. To filter, we transform the daily time series into the frequency domain using a Fast-Fourier Transform, omit frequencies higher than 2 days and lower than 10 days, and then invert the transformation. A similar method was used in Schneider et al. (2015) and Woollings et al. (2016). The North Atlantic storm track is identified using vertically integrated eddy kinetic energy (EKE),

$$\text{EKE}(\varphi, \lambda) = \int \left(\overline{u'^2} + \overline{v'^2} \right) dp/2g, \tag{1}$$

and using vertically averaged meridional eddy temperature fluxes $\left\langle \overline{v'T'} \right\rangle$, where $(\cdot)'$ represents a 2– 10 day bandpass filtered field, $\overline{(\cdot)}$ represents a temporal mean, which in this

study is a seasonal-mean climatology. $\langle(\cdot)\rangle$ represents a mass-weighted vertical average, λ is longitude, and p is pressure, the vertical coordinate. All other symbols have their standard meanings. Unless otherwise stated, vertical averages and integrals span 800–200 hPa.

2.3 Evaluating baroclinicity

Previous authors have sought to understand midlatitude dynamics by using a variety of baroclinicity measures. Here we use the baroclinic MAPE (O'Gorman and Schneider 2008; Mbengue and Schneider 2017). Baroclinic MAPE is a local analog of Lorenz's MAPE (Lorenz 1955). MAPE describes the maximum potential energy that can be converted into kinetic energy from an isentropic redistribution of mass (Lorenz 1955). We define baroclinic MAPE following O'Gorman and Schneider (2008), who used vertical averages of the meridional temperature gradient and static stability. MAPE is given by:

$$\text{MAPE}(\varphi, \lambda) = \frac{p_0 \, L_z^2}{24 \, \Gamma_d}(1 - \overline{p}_t/\overline{p}_s)\left\langle \partial_y \overline{T}\right\rangle^2 \left\langle -\kappa \, (\overline{p} \, \partial_p \overline{\theta})^{-1}\right\rangle, \tag{2}$$

where $L_z = 2000$ km is a constant baroclinic zone width (the baroclinic zone is the region of highest baroclinicity), Γ_d is the dry adiabatic lapse rate, $p_0 = 1000$ hPa is a reference pressure, p_t is the pressure at the tropopause (evaluated using the WMO criterion), p_s is the surface pressure, $y = R\varphi$ is northward distance, θ is potential temperature, and κ is the adiabatic exponent. Equation (2) shows that MAPE can be decomposed into the pressure depth of the troposphere, the square of the meridional temperature gradient, and the inverse of the static stability. We focus on the variability in the static stability to help understand its role in constraining the North Atlantic sector's summer variability.

There are several measures of static stability used in the literature—the form depends on the intended use (for a brief review, see Gates 1961). We use a simple non-dimensional measure of static stability in isobaric coordinates,

$$-\overline{p} \, (\partial_p \overline{\theta})/\overline{\theta} = \kappa \frac{(\Gamma_d - \overline{\Gamma})}{\Gamma_d}, \tag{3}$$

where $\overline{\Gamma}$ is the environmental lapse rate (Lorenz 1957; Gates 1961; Holton 2004). It is a measure of dry stability, however, we believe that this measure of static stability is appropriate because it appears in energy transformations in large-scale dynamics (Lorenz 1955; Phillips 1956; Lorenz 1957). Also, we compare the dry stability to its moist counterpart, which is computed by substituting the vertically-averaged moist adiabatic lapse rate for the dry adiabatic lapse rate in (3), and find that the results do not change dramatically, but the continent-ocean contrast in moist stability is substantially lower

than the dry stability contrast. Nonetheless, we conduct our analysis with the dry stability in order to examine the extent to which dry dynamics account for observed features of the general circulation. Indeed, such an approach was used to quantify the extent to which dry dynamics account for the poleward shifts of storm tracks (Mbengue and Schneider 2013), and to link tropical perturbations to extratropical responses (Mbengue and Schneider 2018). Moist generalizations may be added subsequently.

3 Theory

The dominant variables in the mean available potential energy are the meridional temperature gradient, the static stability, and the pressure depth of the troposphere (O'Gorman and Schneider 2008; Mbengue and Schneider 2018). As a first-order approximation, we ignore changes in the width of the baroclinic zone, which is assumed to be a constant synoptic length scale. If we let $G = \left\langle \partial_y \overline{T}\right\rangle^2$, the square of the meridional temperature gradient; $H = \overline{p}_s - \overline{p}_t$, the pressure depth of the troposphere; and $S = \left\langle \partial_p \overline{\theta}\right\rangle^{-1}$, the reciprocal of the static stability; then from the functional form of MAPE = MAPE $(G, H, S) = \alpha GHS$, where α is a constant, it follows that the linear part of a multivariate Taylor expansion of MAPE is given by:

$$\delta\text{MAPE} \propto SH\delta G + GH\delta S + GS\delta H. \tag{4}$$

An exact decomposition of changes in MAPE is given in Mbengue and Schneider (2017), but (4) suffices for our purposes. One approximate measure of the sensitivity between two quantities is the derivative of one quantity with respect to the other, which is closely related to the slope of the regression line. Thus, the sensitivity of MAPE to the squared meridional temperature gradient is

$$\frac{\delta\text{MAPE}}{\delta G} \propto SH + H\frac{\delta S}{\delta \ln G} + S\frac{\delta H}{\delta \ln G}. \tag{5}$$

To obtain (5), we have divided (4) by δG and rewritten $\delta G/G$ as $\delta \ln G$. In regions where the variations in the reciprocal of the static stability are small relative to the variations in the squared meridional temperature gradients and tropopause height, (5) reduces to,

$$\frac{\delta\text{MAPE}}{\delta G} \propto S\left(H + \frac{\delta H}{\delta \ln G}\right). \tag{6}$$

Equation 6 is an important theoretical result. It shows that the sensitivity of MAPE to G is proportional to S. Hence, regions of higher static stability require larger increases in the meridional temperature gradients for a fixed change in the baroclinicity (MAPE), when compared to regions of

lower static stability. That is, in regions where the variations in static stability are small, we say that the static stability's role is to modulate changes in baroclinicity. In regions where the variations in static stability are large, changes in static stability play a direct role in modifying the baroclinicity [second term on the right hand side of (4)].

The first part of the results investigates how the static stability modulates the baroclinicity; that is, we investigate the implications of (6); while the second part investigates how the variability of static stability controls the variability of the baroclinicity in the North Atlantic sector.

4 Results

4.1 Stability and the modulation of baroclinicity

In this section, we contrast seasonal-mean statistics of tropospheric static stability and the North Atlantic storm track to help identify the sources of seasonal differences in potential predictability. Figure 1 uses mid-to-lower tropospheric stability (1000–400 hPa) because the static stability has the largest direct effect on the growth and evolution of extratropical cyclones in this layer.

Figure 1a shows the climatology of vertically-averaged (1000–400 hPa) seasonal-mean dry and moist static stability. The dry stability is computed using (3), and is depicted in the filled, colored contours; while the moist stability also uses (3) but substitutes the moist adiabat for the dry one; it is shown in the unfilled, gray contours. The figure shows that the two forms of static stability qualitatively agree on the spatial distribution of the seasonal-mean climatology of the static stability. Seasonal changes in land–ocean contrast in moist stability are smaller than the dry stability. The dry stability is greater over land during the wintertime, particularly over the east coast of North America, while it is greater over the North Atlantic ocean during the summertime. The largest summer values are located near Nova Scotia. The land–ocean contrasts in static stability are consistent with a relatively colder boundary layer compared to the overlying air over the land during the winter, and over the ocean during the summer.

Figure 1b shows the interannual variability of vertically-averaged static stability (the coefficient of variation[1] is used to measure the interannual variability and is computed from seasonally-averaged data over the period 1981–2013). Over the baroclinic zone,[2] a standard fluctuation in the static

stability is less than 5% of the point-wise seasonal-mean value. During the wintertime, most of the variability is north of 40°N, particularly around Greenland and near the west coast of Canada. These regions of high coefficient of variation are associated with large horizontal gradients of static stability that are roughly parallel to the zonal-mean wind. The elevated static stability variability off the east coast of Nova Scotia, which extends across the central Atlantic around 50°N is affected by developing cyclones leaving the winter baroclinic zone (compare the left panels of Fig. 1b and the unfilled, gray contours in Fig. 1c, which show the climatology of baroclinic MAPE).

Zonal winds and horizontal gradients of static stability are weaker in summer compared to winter. This partly explains why the variability of static stability in summer is lower than in winter. The region of elevated interannual variability between Iceland and the British Isles during summer is also related to storm-track activity, since storms modify tropospheric stability through their dynamics. The variability of summer static stability is small across the continental region (except over desert regions) and much of the North Atlantic Ocean. Note also that the coefficient of variation of tropospheric static stability achieves a minimum over most of the baroclinic zone.

Figure 1c shows the first EOFs of 400–100 hPa vertically-averaged (upper-level) static stability for DJF and JJA, and contrasts it with the spatial distribution of the climatology of seasonal-mean vertically-averaged baroclinic MAPE (unfilled, gray contours). Upper-level static stability is analyzed because (1) most of the variability in vertically-averaged static stability occurs in the upper troposphere, and (2) it allows us to disentangle the forcing associated with the moist dynamics of the storm track from remotely driven dry-dynamical forcing. These panels show that the leading patterns of variability of the static stability are focused over the ocean in both seasons, where the coefficient of variation is large.

The spatial pattern of static stability (Fig. 1a) suggests that MAPE may exhibit greater sensitivity to temperature gradients over the Atlantic Ocean during winter and over land during summer [i.e., S in (6) is high]. The strong qualitative differences in the dry stability between seasons is another reason we focus on the role of stability in modulating the variability in the North Atlantic sector.

To test this idea, MAPE's sensitivity to changes in the squared meridional temperature gradients is computed for a subset of grid points over land and compared to a subset of ocean-based grid points. The sensitivity is computed using a point-wise linear regression of the seasonal-mean climatology of MAPE onto the seasonal-mean climatology of the squared meridional temperature gradients. Figure 2 shows that the MAPE's sensitivity is greatest over the winter ocean and summer land, where and when the stability

---

[1] The coefficient of variation is computed by dividing the standard deviation by the arithmetic mean.

[2] The baroclinic zone is defined as regions of elevated baroclinicity and can be identified by maxima in the contours of baroclinic MAPE in Fig. 1c.
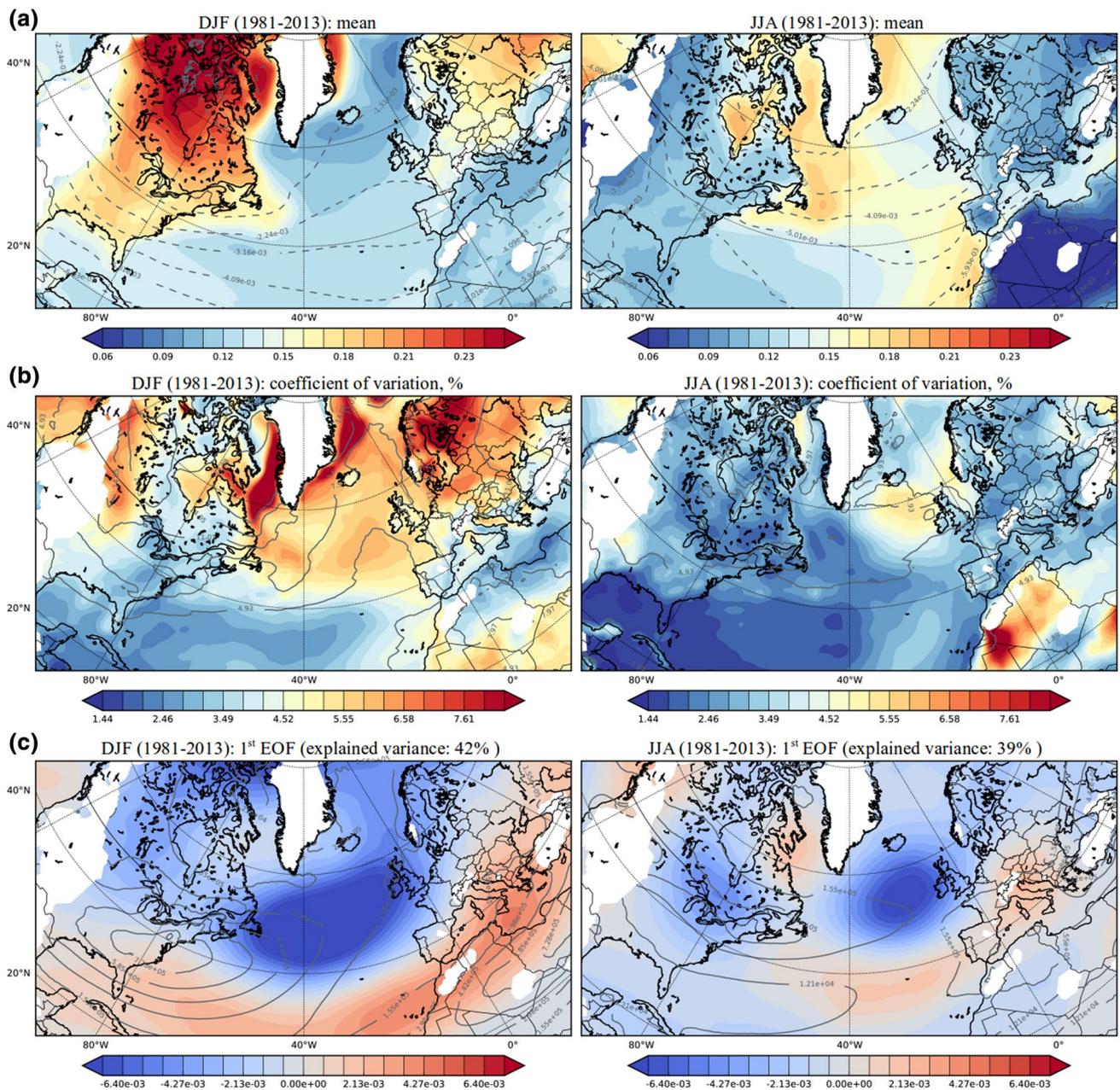
Fig. 1 a The climatology of vertically-averaged (1000–400 hPa) seasonal-mean dry static stability $-\overline{p}\,\partial_p\overline{\theta}/\overline{\theta}$ in the filled contours and moist stability $\left(\Gamma_s - \overline{\Gamma}\right)/\Gamma_s$ in the gray contour lines. $\overline{\Gamma}_s$ is the saturated adiabatic lapse rate. **b** Interannual variability of the dry and moist stability measured using the coefficient of variation computed from seasonal averages of the two static stabilities. **c** The 1st empirical orthogonal function of upper-level seasonal-mean dry static stability (400–100 hPa). The gray contours show the climatology of vertically-averaged seasonal-mean MAPE in units of J/m^2. White colors mark surface pressures greater than an annual climatology (1981–2010) of 900 hPa. Left: DJF. Right: JJA

is at its lowest and as predicted by the theoretical model (6). The decreasing order of sensitivity is as follows: winter ocean, summer land, winter land, and summer ocean. The land-based grid points used in the sensitivity calculation are the ones enclosed by the coordinates (255E–285E, 30N–60N), while the ocean-based grid points are enclosed by (320E–350E, 30N–60N).

The baroclinic MAPE and the storm tracks are slightly offset in the Atlantic sector (the tropospheric jets mostly collocate with MAPE because thermal-wind balance holds in the seasonal mean and MAPE is proportional to the square of the meridional temperature gradient). Figure 3 shows MAPE and 2–10 day bandpass-filtered EKE and meridional eddy fluxes of temperature. The maximum EKE is located
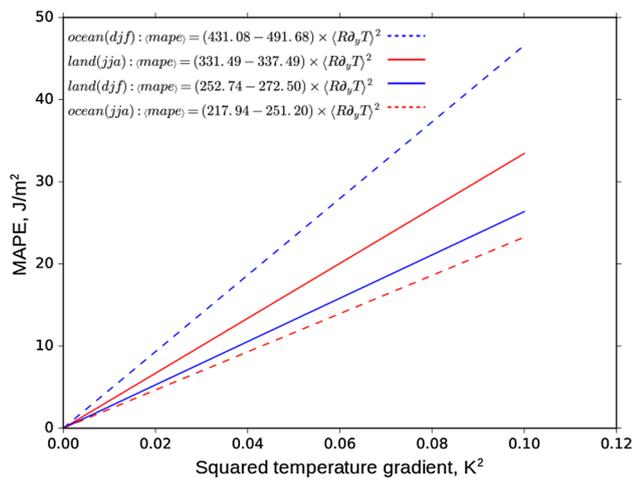
Fig. 2 The sensitivity of MAPE over a subset of land-based grid points (solid lines) and ocean-based grid points (dashed lines) during DJF (blue lines) and JJA (red lines). The text shows the least-squares regression model. The bracketed interval is the 95% confidence interval for the sensitivity of vertically-averaged seasonal-mean MAPE to squared vertically-averaged seasonal-mean meridional temperature gradients.

northeast of the maximum MAPE. This suggests that synoptic-scale storms grow in the baroclinic zone and attain their maxima downstream and poleward of the local baroclinic zone. Atlantic wintertime baroclinicity is greater than summer baroclinicity because wintertime meridional temperature gradients are larger. As a consequence, wintertime EKE is larger. The meridional eddy fluxes of temperature has two maxima in summer: one maximum over the North American continent and one coincident with the winter maximum meridional eddy temperature flux, near to the Gulf Stream. This is evidence of the increased importance of continental baroclinicity during summer. The continental extremum of meridional eddy fluxes of temperature is shifted poleward in summertime compared to the wintertime.

The meridional extent of the summer baroclinic zone is smaller than in winter and is shifted poleward. Similarly, the meridional extent of the maximum contour of EKE is smaller in summer than in winter. By contrast, while the EKE maximum in the Northwest Atlantic shifts poleward, the EKE maximum in the Northeast Atlantic remains somewhat fixed. As a result, the summer storm track is more zonal than the winter storm track. The summer Hadley
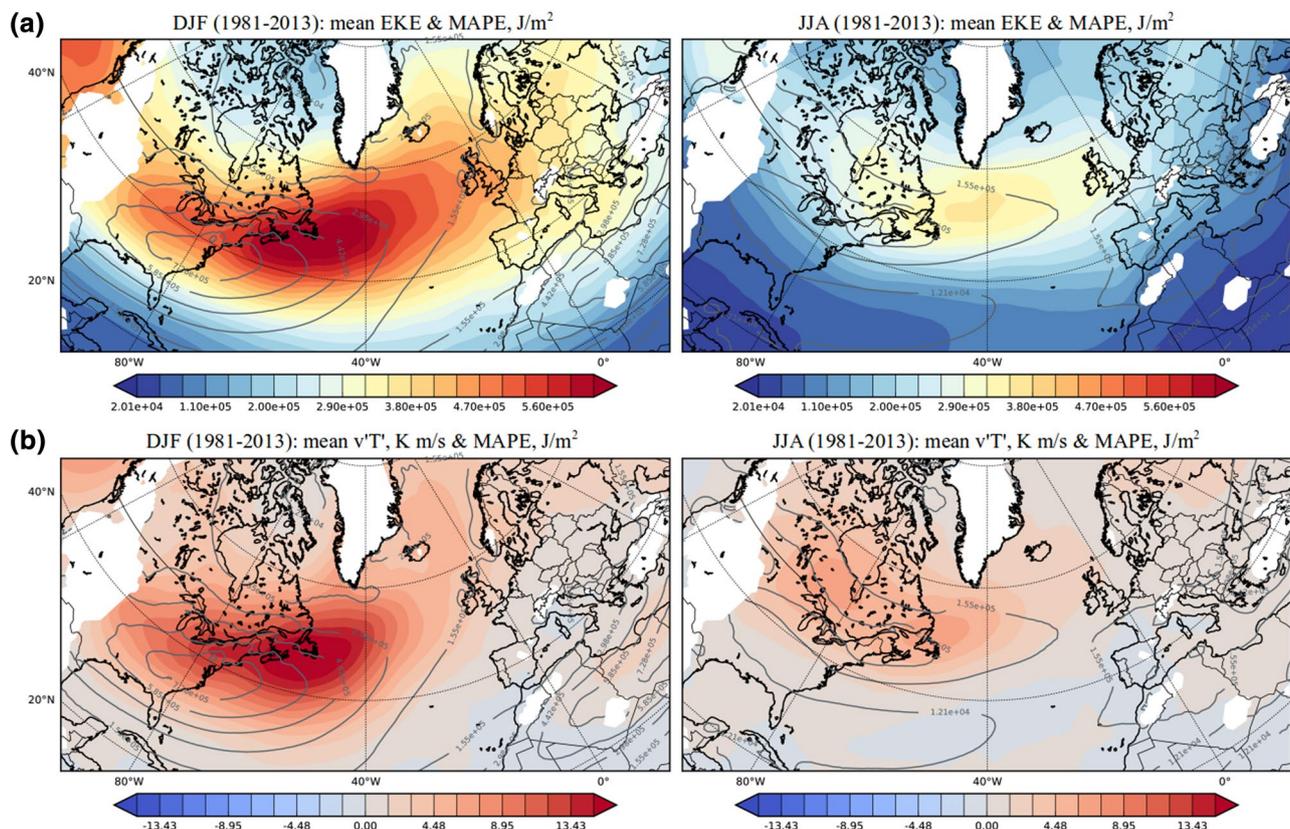

Fig. 3 Climatology of vertically-integrated seasonal-mean baroclinic mean available potential energy (gray, unfilled contours) and, in the filled, colored contours, **a** climatology of vertically-integrated seasonal-mean 2–10 days bandpass-filtered eddy kinetic energy (EKE). **b** Climatology of vertically-averaged seasonal-mean 2–10 days bandpass filtered meridional eddy temperature flux. The vertical composites are composed of data between 800 and 200 hPa. Surface pressures greater than an annual climatology of 900 hPa are colored white. Left: DJF. Right: JJA

cell terminus, which marks the northern-most extent of the descending branch of the Hadley cell, is also farther poleward than the winter terminus (not shown but see Davis and Birner 2013). The poleward-shifted summer Hadley cell is expected to interact more with extratropical eddies than its winter counterpart (Walker and Schneider 2006; Schneider and Bordoni 2008; Bordoni and Schneider 2010; Mbengue and Schneider 2017, 2018). The enhanced summer interaction suggests a possible pathway for variability in the tropical Atlantic to influence extratropical variability in the summertime—although the interaction is two way in general.

4.2 MAPE decomposition

The previous section has shown how stability acts to modulate the sensitivity of MAPE to meridional temperature gradients. Now we decompose MAPE into its components to assess the direct role of static stability in MAPE variability.

Figure 4a shows the 1st EOF of vertically-averaged seasonal-mean MAPE; while Fig. 4b shows the 1st EOF of the 850 hPa zonal winds. The EOFs are computed over the Atlantic to isolate Atlantic variability. The gray, unfilled contours show the climatological fields. The spatial structure of MAPE variability is closely related to the spatial structure of the North Atlantic jet variability. To highlight the similarities, we project the zonal wind anomalies onto the first principal component of MAPE in Fig. 4c, and regress the first principal component of 850 hPa zonal winds onto the first principal component of MAPE in Fig. 4d. The projected patterns are nearly indistinguishable in winter, and the linear regression shows strong association. The downstream displacement of the variability associated with the baroclinicity is one notable difference, and is to be expected, as was mentioned earlier. The variability in the Northeast Atlantic during JJA is less well related, yet the general pattern remains. The magnitude of the interannual variability in JJA is weaker than in DJF. The explained variance of the EOF associated with the jet (DJF: 59% vs JJA: 40%) and the baroclinicity (DJF: 52% vs JJA: 33%) is lower in summer than in winter. The spatial patterns of the summer variability in baroclinicity are similar to those found in the Dong et al. (2013) study. The similarity in the spatial structure of variability between the eddy-driven jet and MAPE suggests that MAPE can be used to understand the Atlantic jet and storm track variability in observations, which is consistent with the conclusions of Mbengue and Schneider (2017).
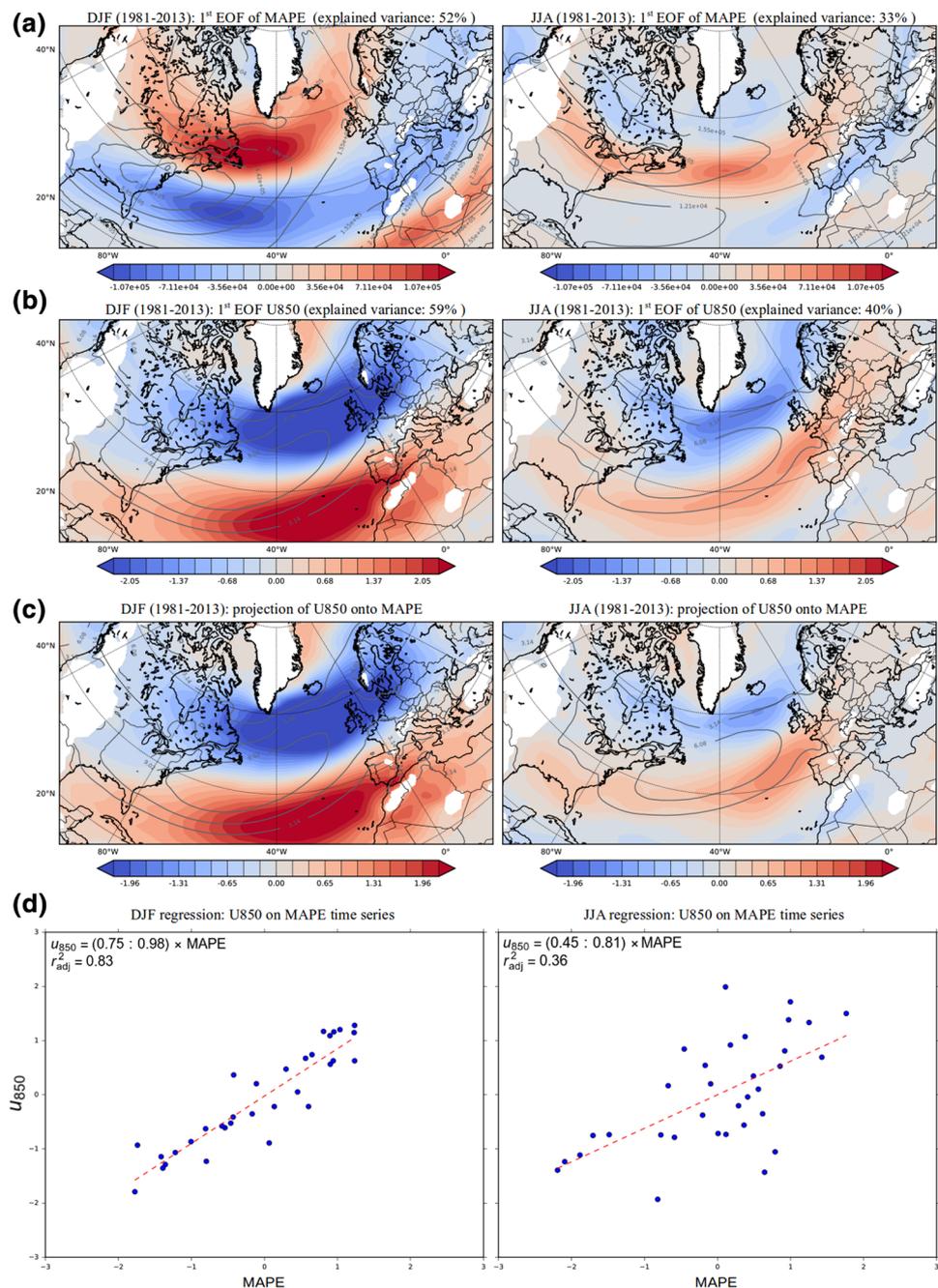
We decompose MAPE into its main components—the static stability and the squared meridional temperature gradients—and show them in Figs. 1 and 5. Figure 5a shows the climatology of squared vertically-averaged seasonal-mean meridional temperature gradients in the filled, colored contours, and coefficient of variation in the unfilled, gray contours. Figure 5b shows the 1st EOF of the squared vertically-averaged meridional temperature gradients, while Fig. 5c shows a regression of the 1st principal component of the 850 hPa zonal winds unto the squared vertically-averaged meridional temperature gradients. The meridional temperature gradients are in units of Kelvin, obtained by multiplying by the Earth's radius. The gray, unfilled contours in Fig. 5b show the climatology of vertically-averaged MAPE. These EOFs give an idea of how variations in the meridional temperature gradients contribute to variations in MAPE. The summer meridional temperature-gradient EOF patters are markedly different from the winter. In summer, the maximum interannual variability in meridional temperature gradients occurs in the East Atlantic. This is in contrast to the winter, in which it occurs in the West Atlantic. The 1st EOF of the meridional temperature gradients is spatially similar to the 1st EOF of MAPE in both seasons, and regression analyses show strong associations. These results suggest that the variance of baroclinicity is dominated by the variance in meridional temperature gradients on the timescales considered in this study.

The spatial structure of the EOFs is shifted poleward during the summertime. Also, the part of the baroclinic zone that is over the North American continent is shifted poleward in the summer. The spatial structure of the 1st EOF of the meridional temperature gradients implies a north–south shift of the baroclinic zone in both seasons. This is consistent with the observed north–south shifts of the eddy driven jet on interannual timescales. The temperature-gradient variability seems to be associated with the variability of both the subtropical and eddy-driven jets because it extends far to the south.

The spatial structure associated with the variability of the upper-level static stability, shown in Fig. 1c, is different from MAPE and the meridional temperature gradients. In contrast to the 1st EOF of the meridional temperature gradients, the static stability's 1st EOF is largely monopolar over the North Atlantic. It represents an extension of the baroclinic zone toward Europe in both seasons. Most of the variability of the vertically-averaged stability results from variability near the tropopause. For this reason, we show the upper-level stability, averaged between 400 and 100 hPa. This is consistent with the result that interannual variability of lower/mid tropospheric stability is small (Fig. 1). Variability in upper-level stability may result from changes in the height of the tropopause or from remotely-excited fluctuations in upper-level potential vorticity. Note also that the center of action of the stability EOF is shifted poleward during the summertime.

(a)

(b)

(c)

(d)

Fig. 4 The filled, colored contours show **a** the 1st EOF of seasonal-mean vertically-averaged baroclinic mean available potential energy (800–200 hPa); **b** the 1st EOF of 850 hPa seasonal-mean zonal wind; **c** the projection of 850 hPa seasonal-mean zonal wind anomalies onto the time series associated with the 1st EOF of the vertically-averaged seasonal-mean baroclinic mean available potential energy. The gray, unfilled contours in **a** show the climatology of the vertically-averaged seasonal-mean MAPE, while the ones in **b**, **c** show the climatology of 850 hPa seasonal-mean zonal wind. The units of MAPE are J/m^2 and zonal winds are m/s. **d** Least squares regression of the 850 hPa seasonal-mean zonal wind's 1st EOF's time series onto vertically-averaged seasonal-mean MAPE's 1st EOF's time series. The time series have been standardized. Left: DJF. Right: JJA

4.3 Impacts of the stability anomaly

Figure 6a shows the climatology of vertically-integrated 2–10 day bandpass-filtered EKE in the unfilled, gray contours, and its 1st EOF in the filled, colored contours. A pulsing pattern is the dominant mode of interannual variability of EKE, although there is evidence of a north–south shift component in the Northeast Atlantic in the summertime.

To understand the potential impact of the upper-level stability anomaly on North Atlantic sector storminess, we project the seasonal anomalies of EKE and 300 hPa zonal winds onto the 1st principal component of the static stability. Figure 6b shows the patterns of eddy kinetic energy variability associated with the 1st EOF of static stability in the filled, colored contours, and the patterns of 300 hPa zonal wind variability associated with the 1st EOF of static stability in the gray, unfilled contours. It is apparent from the figure that north–south shifts of EKE and zonal winds are the dominant modes of variability associated with the stability anomaly. The tripolar pattern of jet variability in the summertime suggests that the subtropical jet variability is also associated with the 1st EOF of the static stability.
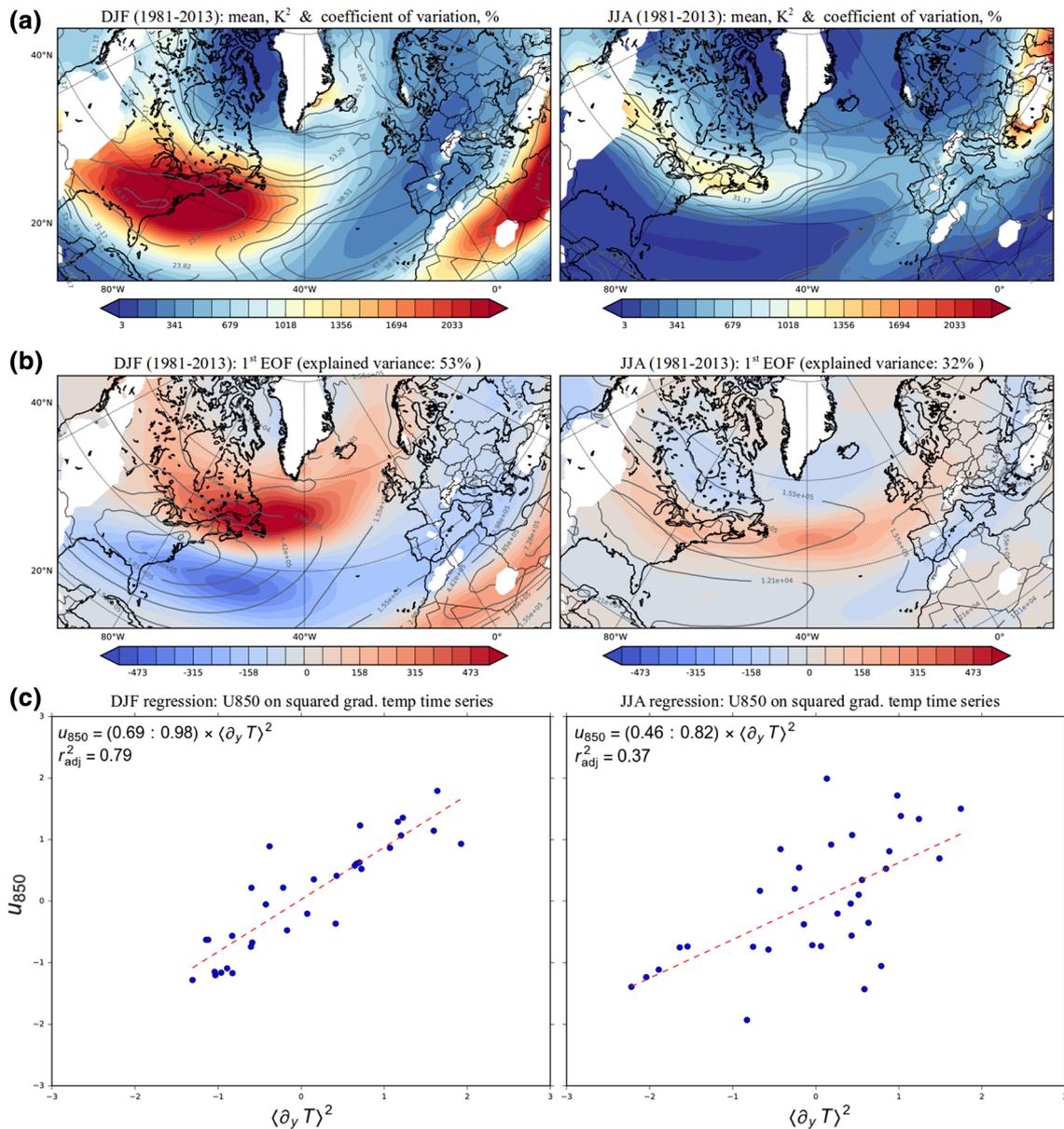
Fig. 5 a The climatology (filled, colored contours) and coefficient of variation (unfilled, gray contours) of the squared vertically-averaged seasonal-mean meridional temperature gradients (800–200 hPa). **b** The 1st EOF of the squared vertically-averaged seasonal-mean meridional temperature gradients (filled, colored contours) and the climatology of the vertically-averaged seasonal-mean baroclinic mean available potential energy (unfilled, gray contours). White colors mark surface pressures greater than an annual climatology of 900 hPa. **c** Least squares regression of the 850 hPa seasonal-mean zonal wind's 1st EOF's time series onto the squared meridional temperature gradients' 1st EOF's time series. The time series have been standardized. Left: DJF. Right: JJA

To compare how synoptic-scale systems interact with the East Atlantic stability variability during the summer, cyclone track densities for each phase of the stability pattern are compared in Fig. 7. The figure shows track density for the negative (left) and positive (right) phases of the summer stability pattern for cyclone tracks that are constrained to (a) emerge from the West Atlantic baroclinic zone and (b) cross into Europe. Only cyclones that genesis in the box (260E–340E, 30N–50N) are considered. All plots have

120 cyclones. They are the 120 most intense cyclones that meet the above criteria over the period 1981–2013. These Lagrangian track statistics corroborate the results obtained using seasonal-mean climatologies. During the negative, low-stability phase, the storm track is shifted poleward and fewer cyclones cross the British Isles. The converse is true during the positive, high-stability phase.

Figure 8 shows a lagged regression of daily England and Wales precipitation and outgoing longwave radiation onto
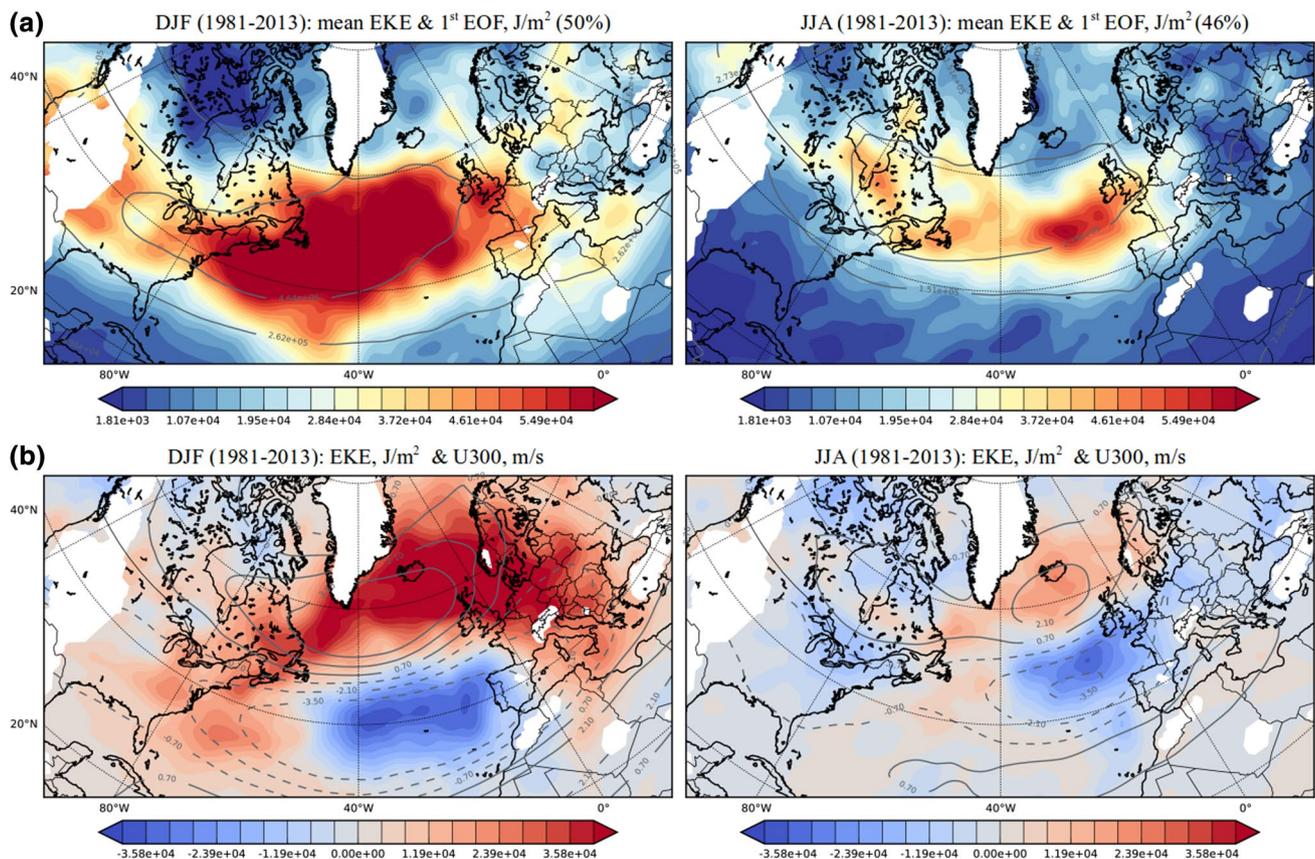
Fig. 6 a The climatology of vertically-integrated seasonal-mean 2–10 days bandpass-filtered eddy kinetic energy (unfilled, gray contours) and its 1st EOF (filled, colored contours). **b** Projection of EKE (filled, colored contours) and 300 hPa zonal winds (unfilled, gray contours) anomalies onto the upper-level stability's 1st EOF's time series. Surface pressures greater than an annual climatology of 900 hPa are colored white. Left: DJF. Right: JJA

the time series of the reciprocal of the static stability during JJA. The vertical green line marks the lead time of the correlation extremum: about 3 days lead. The lag regression shows that during summer, high static stability at upper levels is associated with and leads precipitation and convection (crudely measured using OLR) over the British Isles by about 3 days. Thus, it is more likely that high static stability at upper levels causes an increase in Northeast Atlantic storminess than vice-versa.
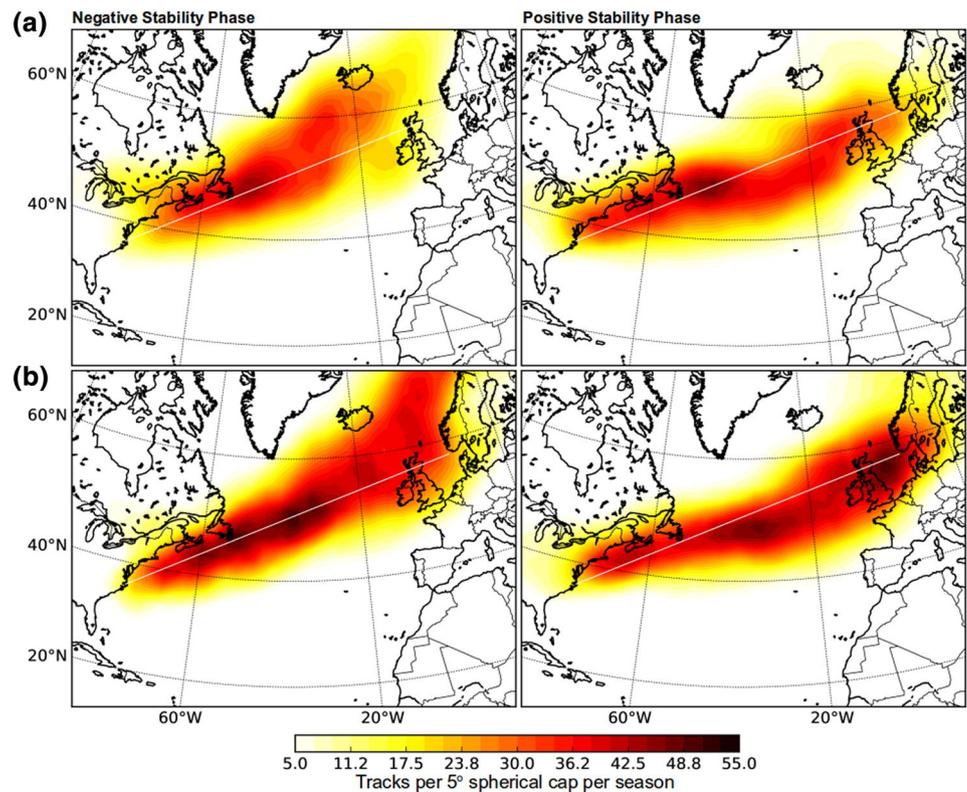
4.4 Comparison to other modes of variability

Figure 9 compares linear regressions of the anomalies of upper-level zonal winds onto the NAO, the dominant mode of variability in the North Atlantic, and the PCs of vertically-averaged squared meridional temperature gradients and upper-level stability. The winter projections for all three are similar, and a multiple linear regression model of the NAO using the components of MAPE explain almost 80% of the variance of the NAO in winter. Therefore, the variability in the meridional temperature gradients and static stability

are strongly related to the variability of the NAO in winter. The extrema of the projected patterns of meridional temperature gradients and of static stability are to the west of the extremum of the projected pattern associated with the NAO. Thus, they are not exactly the same, but are clearly very strongly related. In DJF, the centers of action of the meridional temperature-gradient pattern are shifted to the west of those of the static stability pattern; while in JJA, they coincide over the Atlantic and are to the west of them over North America. This can be interpreted as the static stability playing a greater role in shaping the summer circulation because more of its variability is upstream of the storm track. Furthermore, there is evidence that some of the variability associated with the static stability may be unrelated to the NAO. Indeed, a multiple linear regression model of the summer NAO using the components of MAPE explains less than 20% of the variance of the NAO. Therefore, in summer the mode of variability associated with the upper-level stability anomaly is only weakly associated with the NAO.

To probe the seasonal persistence of the stability anomaly, we assess associations among the seasons using the 1st

Fig. 7 Track density composites for the negative, low-stability (left) and positive, high-stability (right) phases of the summer stability pattern for cyclone tracks that are constrained to **a** emerge from the West Atlantic baroclinic zone, that is those that cross into the box (310E–330E, 30N–60N) and **b** cross into Europe, that is cross into the box (0E–20E, 30N–80N). Only cyclones that genesis in the box (260E–340E, 30N–50N) are considered. All plots have 120 cyclones

EOFs of stability. To do so, we perform seasonal lagged regressions of the 1st principal components of the upper-level stability in the North Atlantic. The lagged regression between the summer and winter static stability PCs shows no statistically significant relationship, but there is a positive and statistically significant relationship between the spring and summer static stabilities—but this explains only about 20% of the variance. Nonetheless, this suggests that if stability acts to reduce the available potential energy during spring, there is a small chance that it may persist through the summer. Finally, no statistically significant relationship between the autumn and winter static stability PCs was found.

4.5 Drivers of the East Atlantic stability anomaly

We have shown that variability associated with the upper-level stability anomaly is important for understanding North Atlantic circulation variability, we now attempt to understand the drivers of the stability anomaly.

Figure 10 shows four linear regressions onto the 1st principal component of upper-level stability in the summer: the zonal winds, the geopotential height, both evaluated at 300 hPa, the outgoing longwave radiation, and the specific humidity averaged between 300 and 100 hPa. The figure suggests that anomalously high stability is associated with upper-level cyclonic circulation, which is consistent with an

upper-level positive potential vorticity anomaly (Fig. 10b). Furthermore, the stability anomaly appears significantly correlated with the suppression of convection throughout the equatorial Atlantic (Fig. 10c). Here, we assess the statistical significance using both the ensemble sensitivity method outlined in Dacre and Gray (2013), which is shown in the intensity of the contours, and the FDR method outlined in Wilks (2016). Statistically significant points at the 90% significance level are shown in the white dots. Consistent with a reduction in tropical Atlantic-wide convection, the stability anomaly is associated with an anomalously dry upper troposphere over the central Atlantic (Fig. 10d). Because convection is the dominant source of tropical upper-tropospheric moisture, these observations suggest a weakening of the tropical Atlantic meridional overturning circulation. This weakening of the overturning circulation may lead to an expansion of the Atlantic Hadley cell and to a poleward shift of the subtropical jet, which can be observed from Fig. 10a, and which can be obtained from theoretical arguments (Walker and Schneider 2006; Frierson et al. 2007; Lu et al. 2007; Korty and Schneider 2008; O'Gorman 2011; Mbengue and Schneider 2013; Levine and Schneider 2015).

There is a statistically significant, positive correlation between the upper-level stability anomaly and convection over the Pacific. Hence, Rossby waves excited in the Pacific may play a role in Atlantic variability. The climatological upper-level zonal winds favor Rossby-wave propagation
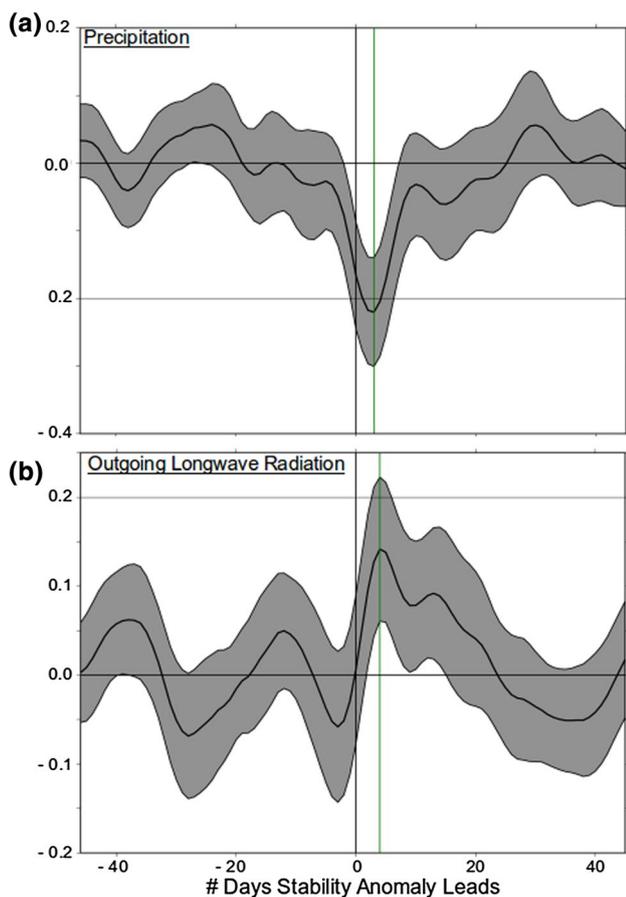
Fig. 8 A lagged correlation of daily summer (JJA) reciprocal of stability (averaged over the region: 40N–55N, 35W–10W, 400 hPa–200 hPa) onto daily England and Wales precipitation (top) and OLR (bottom). The gray shading shows the 95% confidence interval and the vertical green line marks the correlation extremum (about 3 days). Correlations of ± 0.2 are marked with gray horizontal lines

into midlatitudes. Moreover, the regression of the stability anomaly onto the upper-level zonal winds shows that the high stability phase is associated with anomalous zonal winds that are favorable for Rossby-wave propagation. Furthermore, convection over the southeast of North America is significantly related to the stability anomaly. It is possible that upper-level divergences associated with the convection trigger Rossby waves that propagate into the North Atlantic sector. Therefore, we hypothesize that convection over the southeast of North America may play a role in driving some of the variability of summer North Atlantic circulation through the upper-level stability anomaly. Indeed, errors in convection over North America have been identified as a precursor to poor medium-range European forecasts (Rodwell et al. 2013).

The weakening of the Atlantic overturning circulation is notable from Fig. 10c, d. This may be driven by descent caused by convection over the Pacific. The results from the

study of Schwendike et al. (2014) suggest that a Walker-type circulation may contribute to descent over the tropical Atlantic.

Finally, Fig. 10 also implies that variations in the stability anomaly may also occur through changes in the subtropical jet that are forced by changes in the Hadley circulation. As the subtropical jet shifts polewards and increases in magnitude in accordance with the conservation of angular momentum (Fig. 10a), a cyclonic vorticity anomaly occurs to the north, which implies a concomitant increase in upper-level static stability.

5 Discussion

Interannual variations in static stability over the North Atlantic baroclinic zone (Fig. 1b) are lower when compared with variations of the meridional temperature gradients (Fig. 5a). This provides observational evidence for the fact that the seasonal-mean distribution of static stability modulates MAPE's sensitivity to the meridional temperature gradients and to the tropopause height, since in (5), $\delta S \approx 0$. The sensitivity detailed here captures the sensitivity associated with the nonlinear dependence of baroclinicity on temperature (Woollings et al. 2009). To see this explicitly, consider $\overline{T'^2} \propto (\partial_y \bar{T} L_z)^2$ (Held and Larichev 1996; Schneider and Walker 2008; Schneider et al. 2015), since turbulent eddies mix large-scale temperature gradients over a baroclinic region L_z. It then follows that an increase in temperature variance accompanies an increase in mean baroclinicity. Note that the implicit assumption that there exists a separation between the scale of variation of the mean meridional temperature gradient and the eddy length scale holds on Earth.

Our results suggest that the magnitude of the forced response of midlatitude baroclinicity to external drivers, which directly impacts storm-track dynamics, varies seasonally partly because of the differences in the sensitivity of baroclinicity to meridional temperature gradients. The changes in the storm-track activity associated with temperature-gradient variability over the Atlantic Ocean would be greater during the wintertime because baroclinicity over the ocean is more sensitive to temperature-gradient changes during winter (Fig. 2). By contrast, the summer baroclinicity over the North American continent is more sensitive to temperature-gradient changes compared to the winter. Therefore, the summer baroclinicity variability may be more sensitive to the temperature-gradient variability associated with land ice and soil moisture, as was noted by Koster et al. (2011). Similarly, Gulf stream anchoring of the storm track in the West Atlantic may be diminished in summer because of the reduced sensitivity of baroclinicity.

The 1st EOF of upper-level stability represents an eastward extension of the Atlantic baroclinic zone in summer
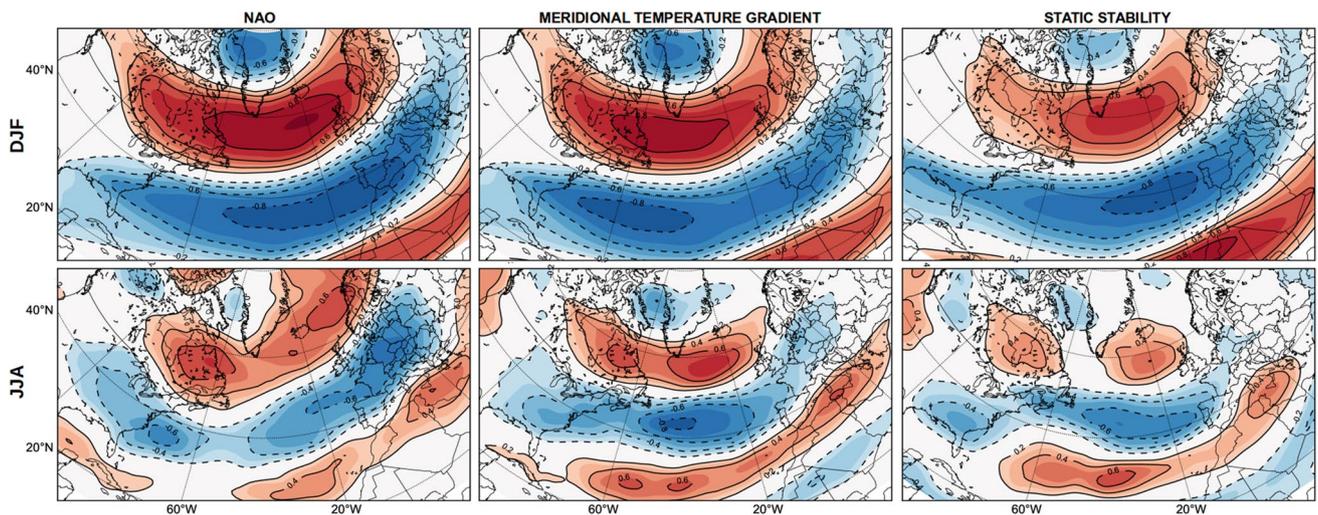
Fig. 9 Linear regression of the anomalies of 300 hPa zonal winds onto the NAO (left), the first principal component of the squared vertically-averaged meridional temperature gradient (middle), and the first principal component of the upper-level stability (right), using seasonally-averaged data (1981–2013). Top: DJF. Bottom: JJA

and winter. The positive phase of the EOF in summer is associated with high stability at upper levels. It may seem counterintuitive that high stability implies higher eddy kinetic energy and storm track density in a region; however, an upper-level positive potential vorticity (PV) anomaly is dynamically consistent with upper-level high static stability and cyclonic rotation. This implies enhanced baroclinicity on the equatorward flank of the anomaly because vertical wind shears increase there.

Ordinarily, it is difficult to determine whether a stability anomaly caused a change in extratropical cyclone activity or a change in extratropical cyclone activity caused a stability anomaly. But rainfall over the British Isles lags the East Atlantic stability anomaly by roughly 3 days, which suggests that the stability anomaly develops first, and that the enhanced baroclinicity leads to an increase in synoptic activity in the East Atlantic. Figure 8b presents more evidence of this since the correlation becomes notably periodic only when the OLR leads the stability anomaly. Since the stability anomaly occurs in the upper troposphere above the level of distributed latent heat release by extratropical cyclones, we have effectively decoupled changes in stability from the moist dynamics of the storm tracks, which are known to influence the spatial distribution of baroclinicity (Hoskins and Valdes 1990; Papritz and Spengler 2015; Woollings et al. 2016). This decoupling allows us to understand the degree to which dry dynamics account for the variability in the stability anomaly. Note that the variability of mid/lower tropospheric static stability (see Fig. 1b) does not show strong interannual variability collocated with the upper-level stability anomaly.

5.1 Potential mechanisms

The correlation between the East Atlantic upper-level stability anomaly and convection over the tropical Atlantic is of interest for several reasons. (1) In the vicinity of the 20W meridian, the meridional overturning circulation is unimpeded by continents. This means that the Hadley cell's return flow could freely evaporate moisture in the subtropics, in contrast to return flow over the African continent. This suggests that convection over the Atlantic ITCZ can be particularly potent and coupled to the extratropics. (2) The summer Hadley cell is displaced poleward (Davis and Birner 2013) and is in a position to perturb and be perturbed by the large-scale extratropical circulation (Schneider and Bordoni 2008). This is because the upper branch of the summer Hadley cell sits inside a region of westerlies, poleward of the critical line of extratropical eddies. The critical line defines the latitude at or before which extratropical eddies break. (3) Previous studies have demonstrated extratropical circulation responses to remote tropical forcing, usually through Rossby wave dynamics. (4) The tropics are more predictable than the extratropics on seasonal timescales and so, tropical drivers of extratropical variability are particularly useful for improving seasonal-to-decadal forecasts. These reasons, along with the strong correlations on interannual time scales (Fig. 10), suggest an alternative mechanism for the stability anomaly: the stability anomaly could be driven by the tropical Atlantic overturning circulation.

Changes in the tropical Atlantic overturning circulation could contribute to the upper-level stability anomaly in at least three ways:
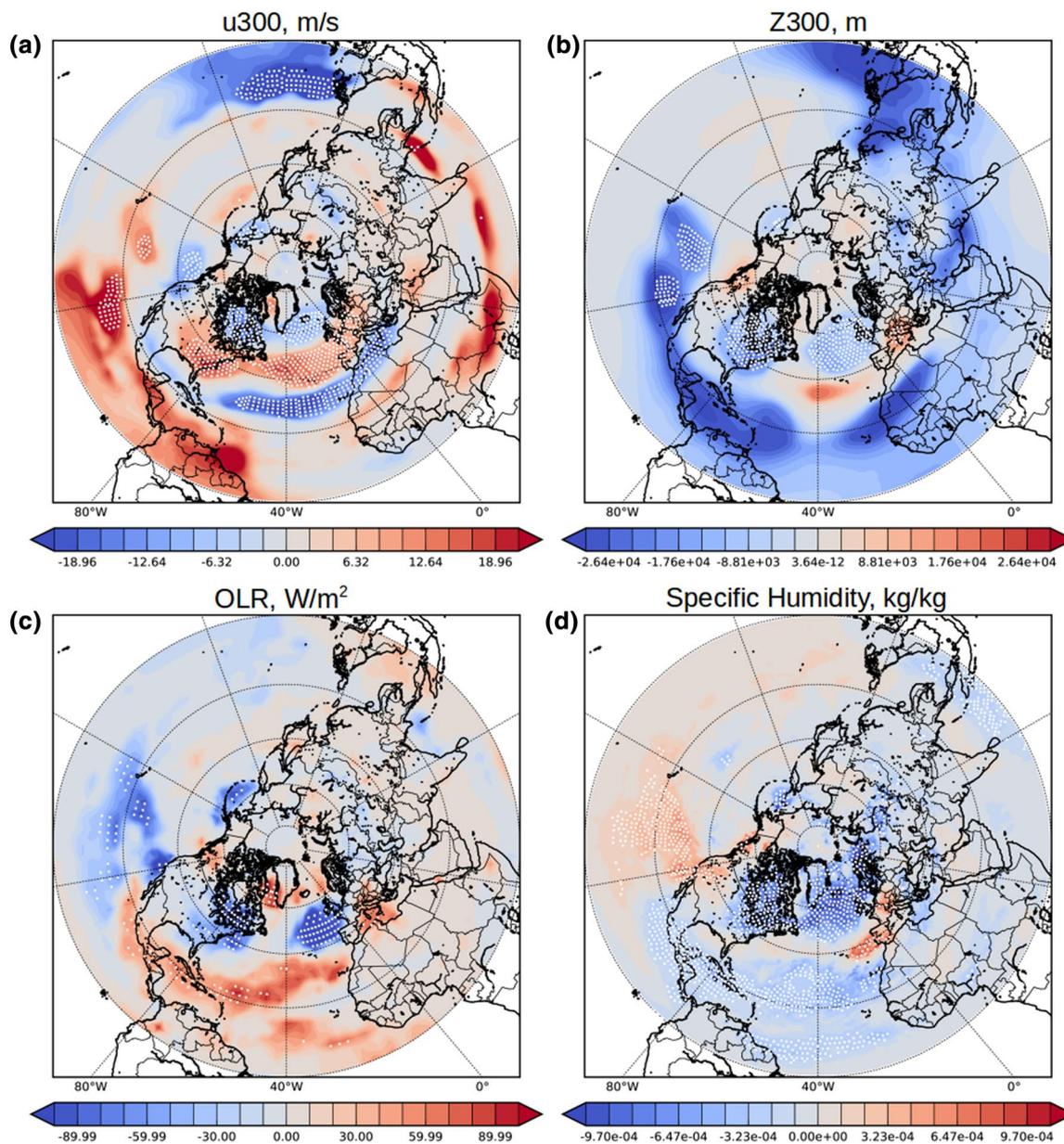
Fig. 10 Sensitivities of vertically-averaged seasonal-mean dry static stability, computed by projecting the following fields' time series onto the static stability's 1st principal component time series: **a** 300 hPa zonal winds, **b** 300 hPa geopotential height, **c** outgoing longwave radiation (OLR), and **d** specific humidity averaged between 300 and 100 hPa. The white dots indicate high statistical significance, while the dark colors show a less-stringent degree of statistical significance

1. For fixed Hadley cell width, changes in cross-equatorial energy fluxes could lead to shifts in the Hadley cell terminus via changes in the position of the ITCZ (see Schneider et al. 2014). Because the Atlantic meridional circulation is confined, an anomalously poleward Hadley cell terminus would manifest as a cyclonic vorticity anomaly in the region of the stability anomaly.

2. Figure 10 suggests that the stability anomaly is also associated with reduced Atlantic convection. If the Hadley circulation terminates where a measure that depends on the static stability and the vertical wind shear exceeds a critical value (Walker and Schneider 2006; Frierson et al. 2007; Lu et al. 2007; Korty and Schneider 2008; Levine and Schneider 2015), then a reduction in the strength of the circulation implies an expanded Hadley cell. If the cause of the reduction in the strength of the Hadley terminus does not simultaneously shift the ITCZ equatorward, then this expansion implies a poleward-shifted Hadley terminus and subtropical jet.

3. A contraction of the local Atlantic meridional overturning circulation could draw high potential-vorticity air into the troposphere leading to the upper-tropospheric stability anomaly. Indeed, equatorward shifts of midlatitude storm tracks associated with contractions of the Hadley cell terminus are well documented (Chang 1995; Tandon et al. 2012).

Therefore, we hypothesize the following mechanism based on the preponderance of the evidence presented in this paper. The anomalous increase in the strength of the local subtropical jet in the East Atlantic induces anomalous cyclonic circulation in the upper troposphere—a positive PV anomaly. This positive PV anomaly, assuming an order unity Burger number, implies that the upper-level stability increases as well. This positive PV anomaly increases east Atlantic baroclinicity through an increase in the vertical wind shear and a dynamically consistent increase in the near-surface meridional temperature gradient. This mechanism reconciles the increase in the upper-level stability that occurs with an increase in synoptic activity in the Northeast Atlantic during the summertime.

5.2 Synthesis with previous studies

The dynamics of Earth's midlatitude atmosphere involve a myriad of drivers. Some drivers act in compensating ways. Here we synthesize our results with some previous work and note alternative mechanisms of the upper-tropospheric stability anomaly.

Gaetani et al. (2011) hypothesize that changes in the meridional overturning circulation associated with convection over the Sahel could drive changes in descent that modify the East Atlantic circulation. Although this is possible during strong monsoons, Fig. 10 suggests that the variability associated with the upper-level stability anomaly in this study has a different source. Note that the Gaetani et al. (2011) study considered the JAS season, while we consider the JJA season.

Upper-tropospheric stability anomalies could be driven by changes in the tropopause height that are related to the stratospheric circulation. For example, an anomalous poleward heat transport in the stratosphere could lead to tropical cooling and midlatitude warming above the tropopause. This would result in a higher tropical tropopause and a lower extratropical tropopause (Haqq-Misra et al. 2011).

Extratropical eddies might contribute to the stability anomaly through dry dynamical effects. However, we have shown that the stability anomaly leads precipitation over the British Isles, which suggests that it precedes extratropical cyclones. Furthermore, little of the interannual variability of tropospheric stability occurs below or upstream of the upper-level stability anomaly. The combined evidence suggests that extratropical eddies are not primarily responsible for the initial incidence of the stability anomaly.

Wang (2002) suggested that Pacific perturbations can be communicated first to the tropical Atlantic through the Walker circulation, and subsequently to the extratropics through changes in the strength of the Hadley circulation. Here we extend this idea and demonstrate that changes in the extent of the Hadley cell also influence North Atlantic variability. Furthermore, perturbations in the strength of the Hadley circulation, which could lead to changes in the extent of the circulation, could have origins in the tropics (Tandon et al. 2012) or in the opposite hemisphere (Baker et al. 2017, 2018).

Finally, the studies of Dacre and Gray (2009, 2013) show differences in the characteristics and precursors of East and West Atlantic cyclones. Furthermore, East Atlantic cyclones have a higher probability of crossing into Europe. The development of East Atlantic cyclones in the absence of a strong near-surface baroclinic zone is an active research subject. For example, it has been suggested that East Atlantic cyclones are primarily secondary cyclones or are beneficiaries of atmospheric preconditioning by antecedent cyclones (Dacre and Gray 2009, 2013). Our results complement their research: we show how the variability of East Atlantic baroclinicity can be driven from the tropics. Since East Atlantic cyclone genesis is primarily driven by mechanisms other than a strongly forced low-level baroclinic zone, tropical Atlantic drivers could contribute to East Atlantic cyclone genesis and growth in the absence of antecedent cyclones.

6 Conclusion

Seasonal forecast skill is lower in summer compared to winter. Here we show, both empirically and theoretically, that the seasonal-mean static stability is inversely proportional to the sensitivity of baroclinicity to meridional temperature gradients in the North Atlantic sector on interannual timescales. Previous studies have shown that the North Atlantic baroclinic zone is more important for developing cyclones than over North America. We show that the lower troposphere over the North Atlantic is more stable in the summertime than in the wintertime. This seasonal difference implies that a unit increase in extratropical meridional temperature gradients results in a larger change in North Atlantic baroclinicity in the wintertime. Using the signal-to-noise ratio as a measure of potential predictability, we find that the difference in the spatial distribution of seasonal-mean static stability constrains potential predictability over the North Atlantic to be lower in summertime compared to the wintertime.

Meridional eddy fluxes of temperature in the North Atlantic sector exhibit two maxima in the summertime: one maximum over North America and one collocated with the

winter maximum flux, near to the Gulf Stream. The North American lower troposphere is less stable in summer and therefore has an enhanced sensitivity of baroclinicity to meridional temperature gradients, which partly explain the summer extremum in meridional eddy fluxes of temperature over North America.

Finally, our analysis of the components of MAPE, a measure of baroclinicity, shows enhanced storminess and an equatorward-shifted storm track over the North Atlantic sector during the positive, high-stability phase of an upper-level static stability anomaly in the summertime. We propose and provide observational evidence for a dynamical mechanism that accounts for this upper-level stability anomaly. The mechanism shows how interannual variability in the tropical Atlantic exerts some control over North Atlantic variability through the tropical meridional overturning circulation. This mechanism enables East Atlantic cyclone genesis in the absence of a strong near-surface baroclinic zone.

References

Alexander LV, Jones PD (2001) Updated precipitation series for the UK and discussion of recent extremes. Atmos Sci Lett. https://doi.org/10.1006/asle.2001.0025

Baker H, Mbengue C, Woollings T (2018) Seasonal sensitivity of the Hadley cell and cross-hemispheric responses to diabatic heating in an idealized GCM. Geophys Res Lett. https://doi.org/10.1002/2018GL077013

Baker H, Woollings T, Mbengue C (2017) Eddy-driven jet sensitivity to diabetic heating in an idealized GCM. J Clim. https://doi.org/10.1175/JCLI-D-16-0864.1

Bengtsson L, Hodges K, Roeckner E (2006) Storm tracks and climate change. J Clim 19:3518–3543

Blackmon M (1976) A climatological spectral study of the 500 mb geopotential height of the Northern Hemisphere. J Atmos Sci 33:1607–1623

Blackmon M, Wallace J, Lau N, Mullen S (1977) An observational study of the Northern Hemisphere wintertime circulation. J Atmos Sci 34:1040–1053

Bordoni S, Schneider T (2010) Regime transitions of steady and time-dependent Hadley circulations: comparison of axisymmetric and Eddy-permitting simulations. J Atmos Sci 67:1643–1654

Chang EKM (1995) The influence of Hadley circulation intensity changes on extratropical climate in an idealized model. J Atmos Sci 55:2006–2024

Charney JG (1947) The dynamics of long waves in a baroclinic Westerly current. J Meteorol 4(5):135–162

Dacre HF, Gray SL (2009) The spatial distribution and evolution characteristics of North Atlantic cyclones. Mon Weather Rev 137(1):99–115

Dacre HF, Gray SL (2013) Quantifying the climatological relationship between extratropical cyclone intensity and atmospheric precursors. Geophys Res Lett 40(10):2322–2327. https://doi.org/10.1002/grl.50105

Davis NA, Birner T (2013) Seasonal to multidecadal variability of the width of the tropical belt. J Geophys Res Atmos 118:7773–7787. https://doi.org/10.1002/jgrd.50610

Dee DP et al (2011) The ERA-interim reanalysis: configuration and performance of the data assimilation system. Q J R Meteorol Soc 137:553–597. https://doi.org/10.1002/qj.828

Dong B, Sutton RT, Woollings T, Hodges K (2013) Variability of the North Atlantic summer storm track: mechanisms and impacts on European climate. Environ Res Lett 8(3):034–037

Eady ET (1949) Long waves and cyclone waves. Tellus 1:33–52

Frierson DMW, Lu J, Chen G (2007) Width of the Hadley cell in simple and comprehensive general circulation models. Geophys Res Lett 34:L18804. https://doi.org/10.1029/2007GL031115

Gaetani M, Pohl B, Douville H, Fontaine B (2011) West African monsoon influence on the summer Euro-Atlantic circulation. Geophys Res Lett 38:L09705. https://doi.org/10.1029/2011GL047150

Gates WL (1961) Static stability measures in the atmosphere. J Meteorol 18(4):526–533. https://doi.org/10.1175/1520-0469(1961)018<0526:SSMITA>2.0.CO;2

Haqq-Misra J, Lee S, Frierson DMW (2011) Tropopause structure and the role of eddies. J Atmos Sci 68(12):2930–2944. https://doi.org/10.1175/JAS-D-11-087.1

Held IM, Larichev VD (1996) A scaling theory for horizontally homogeneous, baroclinically unstable flow on a beta plane. J Atmos Sci 53(7):946–952. https://doi.org/10.1175/1520-0469(1996)053<0946:ASTFHH>2.0.CO;2

Hodges KI (1995) Feature tracking on the unit sphere. Mont Weather Rev 123(12):3458–3465. https://doi.org/10.1175/1520-0493(1995)123<3458:FTOTUS>2.0.CO;2

Hodges KI (1999) Adaptive constraints for feature tracking. Mon Weather Rev 127:1362–1373

Holton J (2004) An introduction to dynamic meteorology, 4th edn. Elsevier Academic Press, MA

Hoskins B (2013) The potential for skill across the range of the seamless weather-climate prediction problem: a stimulus for our science. Q J R Meteorol Soc 139(672):573–584. https://doi.org/10.1002/qj.1991

Hoskins B, Hodges K (2002) New perspectives on the Northern Hemisphere winter storm tracks. J Atmos Sci 59:1041–1061

Hoskins BJ, Valdes PJ (1990) On the existence of storm-tracks. J Atmos Sci 47:1854–1864

Korty RL, Schneider T (2008) Extent of Hadley circulations in dry atmospheres. Geophys Res Lett 35:l23803. https://doi.org/10.1029/2008GL035847

Koster RD et al (2011) The second phase of the global land–atmosphere coupling experiment: soil moisture contributions to subseasonal forecast skill. J Hydrometeorol 12(5):805–822. https://doi.org/10.1175/2011JHM1365.1

Levine X, Schneider T (2015) Baroclinic eddies and the extent of the Hadley circulation: an idealized GCM study. J Atmos Sci 72:2744–2761. https://doi.org/10.1175/JAS-D-14-0152.1

Liebmann B, Smith CA (1996) Description of a complete (interpolated) outgoing longwave radiation dataset. Bull Am Meteorol Soc 77:1275–1277

Lorenz EN (1957) Static stability and atmospheric energy. Sci. Rep. No. 9, General Circulation Project, M.I.T., A.F. 19 (604)1000

Lorenz E (1955) Available potential energy and the maintenance of the general circulation. Tellus VII 2:157–167

Lu J, Vecchi AG, Reichler T (2007) Expansion of the Hadley cell under global warming. Geophys Res Lett. https://doi.org/10.1029/2006GL028443

Mbengue C, Schneider T (2013) Storm track shifts under climate change: what can be learned from large-scale dry dynamics. J Clim 26:9923–9930

Mbengue C, Schneider T (2017) Storm-track shifts under climate change: toward a mechanistic understanding using baroclinic mean available potential energy. J Atmos Sci 74:93–110. https://doi.org/10.1175/JAS-D-15-0267.1

Mbengue C, Schneider T (2018) Linking Hadley circulation and storm tracks in a conceptual model of the atmospheric energy balance. J Atmos Sci 75:841–856

McGraw MC, Barnes EA (2016) Seasonal sensitivity of the Eddy-driven jet to tropospheric heating in an idealized AGCM. J Clim 29(14):5223–5240. https://doi.org/10.1175/JCLI-D-15-0723.1

Mesquita MDS, Gunnar Kvamsto N, Sorteberg A, Atkinson DE (2008) Climatological properties of summertime extra-tropical storm tracks in the northern hemisphere. Tellus A 60(3):557–569. https://doi.org/10.1111/j.1600-0870.2008.00305.x

O'Gorman P (2011) The effective static stability experienced by eddies in a moist atmosphere. J Atmos Sci 68:75–90

O'Gorman P, Schneider T (2008) Energy of midlatitude transient eddies in idealized simulations of changed climates. J Clim 21:5797–5806

Palmer TN, Anderson DLT (1994) The prospects for seasonal forecasting—a review paper. Q J R Meteorol Soc 120(518):755–793. https://doi.org/10.1002/qj.49712051802

Papritz L, Spengler T (2015) Analysis of the slope of isentropic surfaces and its tendencies over the North Atlantic. Q J R Meteorol Soc 141(693):3226–3238. https://doi.org/10.1002/qj.2605

Phillips N (1956) The general circulation of the atmosphere: a numerical experiment. Q J R Meteorol Soc 82(352):123–164

Rodwell MJ et al (2013) Characteristics of occasional poor medium-range weather forecasts for Europe. Bull Am Meteorol Soc 94(9):1393–1405. https://doi.org/10.1175/BAMS-D-12-00099.1

Schneider T, Bordoni S (2008) Eddy-mediated regime transitions in the seasonal cycle of a Hadley circulation and implications for monsoon dynamics. J Atmos Sci 65:915–934

Schneider T, Walker C (2008) Scaling laws and regime transitions of macroturbulence in dry atmospheres. J Atmos Sci 65:2153–2173

Schneider T, Bischoff T, Potka H (2015) Physics of changes in synoptic midlatitude temperature variability. J Clim 28(6):2312–2331

Schneider T, Bischoff T, Haug GH (2014) Nature 513

Schwendike J, Govekar P, Reeder MJ, Wardle R, Berry GJ, Jackob C (2014) Local partitioning of the overturning circulation in the tropics and the connection to the Hadley and Walker circulations. J Geophys Res Atmos 119:1322–1339. https://doi.org/10.1002/2013JD020742

Simpson IR, Shaw TA, Seager R (2014) A diagnosis of the seasonally and longitudinally varying midlatitude circulation response to global warming. J Atmos Sci 71(7):2489–2515

Tandon NF, Gerber EP, Sobel AH, Polvani LM (2012) Understanding Hadley cell expansion versus contraction: Insights from simplified models and implications for recent observations. J Clim 26:4304–4321

Walker CC, Schneider T (2006) Eddy influences on Hadley circulations: simulations with an idealized GCM. J Atmos Sci 63(12):3333–3350

Wang C (2002) Atlantic climate variability and its associated atmospheric circulation cells. J Clim 15(13):1516–1536. https://doi.org/10.1175/1520-0442(2002)015<1516:ACVAIA>2.0.CO;2

Wang B et al (2009) Advance and prospectus of seasonal prediction: assessment of the APCC/CLIPAS 14-model ensemble retrospective seasonal prediction (1980–2004). Clim Dyn 33(1):93–117. https://doi.org/10.1007/s00382-008-0460-0

White G (1982) An observational study of the northern hemisphere extratropical summertime general circulation. J Atmos Sci 39(1):24–40. https://doi.org/10.1175/1520-0469(1982)039<0024:AOSOTN>2.0.CO;2

Wilks DS (2016) The stippling shows statistically significant grid points: how research results are routinely overstated and overinterpreted, and what to do about it. Bull Am Meteorol Soc 97(12):2263–2273. https://doi.org/10.1175/BAMS-D-15-00267.1

Woollings T, Hoskins B, Blackburn M, Hassell D, Hodges K (2009) Storm track sensitivity to sea surface temperature resolution in a regional atmosphere model. Clim Dyn 35(2):341–353. https://doi.org/10.1007/s00382-009-0554-3

Woollings T, Hannachi A, Hoskins B (2010) Variability of the North Atlantic Eddy-driven jet stream. Q J R Meteorol Soc 136(649):856–868. https://doi.org/10.1002/qj.625

Woollings T, Papritz L, Mbengue C, Spengler T (2016) Diabatic heating and jet stream shifts: a case study of the 2010 negative North Atlantic oscillation winter. Geophys Res Lett 43(18):9994–10002. https://doi.org/10.1002/2016GL070146

Yin J (2005) A consistent poleward shift of the storm track in simulations of 21st-century climate. Geophys Res Lett 32:L18–701. https://doi.org/10.1029/2005GL023684